Journal Name

ARTICLE

Sustainable metal-free carbogels as oxygen reduction electrocatalysts

Received 00th January 20xx,
Accepted 00th January 20xx

DOI: 10.1039/x0xx00000x

www.rsc.org/

K. Preuss,[a,b] L. C. Tănase,[c] C. M. Teodorescu,[c] I. Abrahams[b,d] and M.-M. Titirici*[a,b]

Tuneable nitrogen doped carbogels have been synthesised by a simple one-pot hydrothermal carbonisation, followed by pyrolysis at 1000 °C, using highly available and low cost precursors such as glucose and ovalbumin as precursors. Different physical activation ratios of nitrogen/oxygen were used to demonstrate a sustainable and easy method for changing surface area, pore size and elemental composition in order to investigate their effect on the oxygen reduction reaction when used as electrocatalysts. A ratio of nitrogen mixed with 2% of oxygen was found to be most beneficial for enhancing the catalytic activity by creating a high surface area of 874 $m^2 g^{-1}$ as well as a favourable ratio of pyridinic to graphitic nitrogen. The influence of sulphur doping and/or boron on the carbogel structure was investigated. Incorporation of sulphur does not interfere with the structure formation, but decreases the surface area and nitrogen content resulting in diminished ORR performance. However, boron doping with boric acid results in a different carbogel structure by acting as a catalyst, creating an altered morphology, surface area, pore properties and higher nitrogen content by fully utilising ovalbumin as a nitrogen source instead of as a structure directing/surface stabilising agent. Nitrogen content is found to determine the limiting current, while the oxygen content has a small influence on the onset potential. An assumed synergistic effect between nitrogen and boron generates higher electron transfer numbers and lower hydrogen peroxide yields in boron nitrogen co-doped carbogels than those observed in purely nitrogen doped systems.

Introduction

Satisfying the ever-increasing demand for energy has become a major challenge for today's society. Obtaining energy from renewable resources is viewed as a desired alternative to conventional sources to avoid increases in carbon dioxide emissions. Polymer membrane electrolyte fuel cells (PEMFCs) represent a promising approach for various automotive, stationary and portable power applications. The cost of these devices is a limiting factor in their widespread commercialisation. The use of Platinum as a catalyst at both anode and cathode is the main reason for this high cost. Apart from its low availability and resources, Pt has shortcomings, such as slow kinetics for the oxygen reduction reaction (ORR) as well as low durability and stability.[1,2] In recent years significant research effort has gone into either reducing the platinum content or completely replacing it by non-noble metals or metal-free alternatives, especially at the cathode.[3–6] It has to be emphasised that the term "metal-free" should be used with care as it has been shown that even the smallest traces of metals like Fe, Ni or Mn can drastically boost the activity of a supposedly metal-free catalyst.[7,8] These traces can either originate from metal salts used during the synthesis or from the metal impurities present in the precursor used for carbonisation. Heteroatom doped carbons have become increasingly popular as metal-free ORR catalysts, where nitrogen doping is the most commonly used either solely or in combination with other heteroatoms such as S and B. A great amount of research has been conducted to investigate the active sites in these metal-free catalysts. Most theories are based on the difference in electronegativity and/or atomic size of the heteroatom compared to carbon which are believed to create positively/negatively charged defects causing polarisation of the neighbouring carbon atoms, which promotes oxygen adsorption and subsequent reduction.[9] The incorporation of nitrogen into the carbon framework can improve electron donation and/or increase basicity to promote oxygen adsorption.[10] However, controversy is caused by the involvement of different nitrogen species. Some researchers suggests that pyridinic N is responsible for the enhanced ORR activity, due to its ability to offer a lone electron pair,[3,11] while others deem it is graphitic N, due to its extra electron in the delocalised π-system.[3,12] Yet others believe the enhanced ORR activity is due to interaction of both pyridinic and graphitic nitrogen.[13] Co-doping nitrogen and sulphur can create a charge density profile and structural defects within the carbon framework on top of an increased polarisability due to lone pairs on sulphur, making interaction with molecules in the electrolyte easier, due to its difference in size (S is a larger atom

[a] School of Engineering and Materials Science, Queen Mary University of London, Mile End Road, E1 4NS London, United Kingdom. Email: m.m.titirici@qmul.ac.uk
[b] Materials Research Institute, Queen Mary University of London, Mile End Road, E1 4NS London, United Kingdom.
[c] National Institute of Materials Physics, Atomistilor 405A, 077125 Măgurele-Ilfov, Romania.
[d] School of Biological and Chemical Sciences, Queen Mary University of London, Mile End Road, E1 4NS London, United Kingdom.
Electronic Supplementary Information (ESI) available.See DOI: 10.1039/x0xx00000x

than N or C) and electronegativity (N is more electronegative than S and C).[4,14,15] By incorporating nitrogen and boron within a network of conjugated carbon atoms, a disruption in uniformity of the charge distribution is created due to the significantly lower electronegativity of B, making it an electron donor that acts as a bridge for the electrons transferring to oxygen, which can weaken O-O bonds.[3] Synthesising metal-free catalysts from sustainable resources, like plant biomass or food waste has shown promising results, though reproducibility due to changing composition presents an issue.[16–18] Relating to this, biomass precursors such as glucose, cellulose or proteins, which can be obtained from biomass, offer a reliable alternative as starting materials for sustainable ORR catalysts. Carbon aerogels made from bacterial cellulose,[19] glucose and phloroglucinol,[20] or glucose and borax[21,22] have been reported with good catalytic activity and stability. A simple one-pot synthesis route for nitrogen doped carbon aerogels based on hydrothermal carbonisation (HTC) of an aqueous solution made from glucose and protein (ovalbumin) was first reported by White et al.,[23] based on earlier research carried out by Baccile et al.[24] These aerogels have later been reported as promising ORR catalyst by Wohlgemuth et al.,[14] who added additional S doping, and Alatalo et al.[25] who used soy protein instead of ovalbumin. The HTC of pure glucose typically results in microspherical non porous carbon by isomerisation of glucose to fructose followed by dehydration to hydroxymethylfurfural (HMF) and other products which then polymerise/nucleate.[26] With the addition of a protein during the HTC as nitrogen source and at the same time a structure directing/surface stabilising agent during the evolution of the hydrothermal carbon network is provided, creating a crosslinked structure.[23] The formation of these aerogels is based on a cascade of reactions classified as Maillard reactions between a reducing sugar and an amine (amino groups of the protein).[27]

Following on previous work,[14,21,23] here we investigate metal free nitrogen doped carbogels synthesised from inexpensive model precursors glucose and ovalbumin and systematically investigate the influence of morphology, surface area and pore properties on their electrocatalytic activity to clarify the most important parameters affecting the ORR catalytic activities on metal free carbon catalysts. For this, the influence of physical activation with oxygen will be studied to present a sustainable and simple method for tuning surface area, pore sizes and elemental composition. We further show how additional heteroatom doping with sulphur and/or boron can change the materials structure and thus enhance or diminish ORR performance due to elemental changes and synergistic effects.

Experimental

Synthesis

All chemicals were purchased from Sigma Aldrich and used as received. Samples were produced via hydrothermal carbonisation of D-(+)-Glucose and lyophilised ovalbumin (OvA) from chicken egg white containing no metal traces, at 180 °C for 5.5 h, as originally described by White et al.[24] For a typical experiment, 1.5 g glucose was mixed with 0.3 g ovalbumin and dissolved in 13.5 g deionised water by sonicating for 30 min. If doping was desired, 1 mmol of the sulphur (2-thiophenecarboxaldehyde/ TCA) and/or boron (boric acid /BA) source was added. The mixtures were prepared in glass vials, which were placed in Teflon inlets and transferred to stainless steel autoclaves (Parr Instruments). After the hydrothermal carbonisation samples were washed by stirring in deionised H_2O for 24 h followed by vacuum filtration and freeze drying for 24 h to yield the cryogel. Subsequently the dried powders were placed in ceramic crucibles, covered with a ceramic lid and placed in a Carbolite tube furnace followed by 15 min of flushing with an N_2/O_2 mixture (nitrogen mixed with compressed air to correspond 1, 2 or 4 % oxygen content). Samples were heated under the appropriate N_2/O_2 mixture at a heating rate of 7 °C/min up to 1000 °C, with a dwell time of 2 h and subsequent cooling to room temperature to yield the carbogels. Yield calculations are based on the mass before and after the pyrolysis process. Sample names are abbreviated as $CN_{dopants}$, indicating the nitrogen doped carbon, as the pure carbogel form and added dopants (S/B). Thus, CN_S notes a nitrogen carbogel, carbonised at 1000 °C, doped with sulphur.

Physical characterisation

Micrograph images were obtained with a FEI Quanta 3D Scanning Electron Microscope (SEM) and a JEOL JEM-2010 Transmission Electron Microscope (TEM). Surface area and pore size distribution/pore volumes (V_{tot}, V_{micro}, V_{meso}) were determined with Brunauer-Emmett-Teller (BET) theory and non-local density functional theory (NLDFT), respectively, using Nitrogen sorption isotherms obtained at 77 K with a Quantachrome Nova 4200e. X-Ray Photoelectron Spectroscopy (XPS) was performed in an AXIS Ultra DLD (Kratos Surface Analysis) setup equipped with an 180° hemispherical electron energy analyser, using Al $K_{\alpha 1}$ radiation (1486.74 eV) produced by a monochromatised X-Ray source at an operating power of 300 W (15kV × 20mA). Charging effects were compensated by a neutralizer. The binding energy scale was calibrated to the C 1s standard value of 284.6 eV. XPS data analysis (fitting procedure) was performed with pseudo-Voigt profiles and associated inelastic backgrounds. For comparison, elemental analysis of the bulk material was carried out for two samples of C, H and N with a Thermo Scientific FlashEA 1112 Series.

Electrochemical characterisation

Electrochemical testing was carried out with a rotating ring disk electrode (RRDE) on a Metrohm Multi Autolab M101. A three-electrode configuration with Ag/AgCl as a reference electrode, platinum as a counter electrode, and glassy carbon with a Pt ring as a working electrode was used. Samples were compared to a commercially available platinum standard (HiSPEC 9100, 60 wt% Pt on carbon). The mass loading for all carbogels on the electrode was kept at 106 μg cm^{-2} and 20 μg_{Pt} cm^{-2} for the Pt standard, respectively. Testing was performed in 0.1 M KOH, where the electrolyte was first purged with N_2 for 30 min and Cyclic Voltammetry (CV) carried out at a scan rate of 100 mV s^{-1},

followed by purging with O_2 for another 30 min. A further CV scan was carried out followed by Linear Sweep Voltammetry (LSV) at a scan rate of 10 mV s^{-1} at 1600 rpm. To calculate the electron transfer number and the H_2O_2 yield, the measured currents on the disk I_D and the ring I_R and the collection efficiency N of the Platinum ring (25 %) were used.

$$\%(H_2O_2) = 200 \times \frac{I_R/N}{I_D+I_R/N} \qquad n = 4 \times \frac{I_D}{I_D+I_R/N}$$

For stability/durability testing a chronoamperic profile was run for 10000 s, where a constant potential of -0.25 V (V vs Ag/AgCl) was applied and the change in current was recorded.

Results and discussion

Tunable nitrogen carbogels were synthesised as sustainable catalysts for the oxygen reduction reaction based on a synthesis route initially described by White et. al.[14,23] The influence of different oxygen activation ratios and dopants was investigated on the morphology, surface area and pore properties as well as the catalytic performance of the carbogels.

Influence of O_2 activation

Optimising surface area, pore properties and other surface groups of carbons is commonly done by activation during the high temperature carbonisation. This can either be achieved via physical (CO_2 or steam) or chemical activation, which usually employs harsh chemicals (i.e. KOH, H_3PO_4), requiring a purification step to remove those from the sample afterwards. Physical activation presents a gentler way of creating surface area, though in the case of O_2 gas at the cost of yield loss and incorporated oxygen containing surface groups. Based on the concept of sustainability we investigate how O_2 activation can be employed to influence the surface area, pore properties and catalytic performance of a nitrogen doped carbogel, by carbonisation under different N_2/O_2 ratios at 1000 °C. For this, samples were either carbonised under pure nitrogen atmosphere or under a mixture of nitrogen and compressed air with ratios of 1, 2 or 4 % of oxygen. Scanning electron micrographs (Figure 1) show similar morphologies for all samples, suggesting that the different activation ratios only affect the sample's microstructure. BET surface areas, pore volumes and yields can be seen in Table 1 (N_2 sorption isotherms can be found in ESI). As expected, the surface area only increases marginally after the carbonisation under inert N_2 atmosphere from 101 m^2 g^{-1} to 110 m^2 g^{-1}, though shifting from larger mesopores to micro- and small mesopores, thus reducing the total pore volume. With increasing oxygen content during carbonisation, surface area increases, while the percentage yield decreases due to an increase in the amount of sample burning off in the presence of oxygen. This phenomenon can be described as *hole burning* due to the oxidation of the carbon surface.[28] Studies in the 1980's and 90's,[29–31] observed that O_2 gas can act as an etching agent to remove carbon atoms from the basal plane leaving voids and creating carbon monoxide and carbon dioxide.[32] Chu and Schmidt[31,33] showed that temperature conditions and gas pressure can influence this *hole burning* process. While at lower temperatures, etching initiates exclusively on already existing point defects, at higher temperatures additional new defect sites are created in the basal carbon plane. Originating from these point defects, monolayer pit formation creates holes/pores (corresponding to micro- and small mesopores). Additionally, line defects can create multilayer pit growth (corresponding to meso- and macropores). This pit growth tends to be hexagonal at lower gas pressures and becomes circular at high pressures.[31] Based on these findings, it can be concluded that an increase in oxygen content also leads to an increase in surface area as well as micro- and mesopore volume. Similar to our materials surface area, the total pore volume also increases with increasing oxygen content, with the exception of CN-2% O_2 showing a slightly lower mesopore volume than CN-1% O_2, due to its higher micropore content. Pore size distributions for the carbonised samples as well as for a cryogel after hydrothermal carbonisation (Figure 2) are in good agreement with the surface area and pore volumes in Table 1.

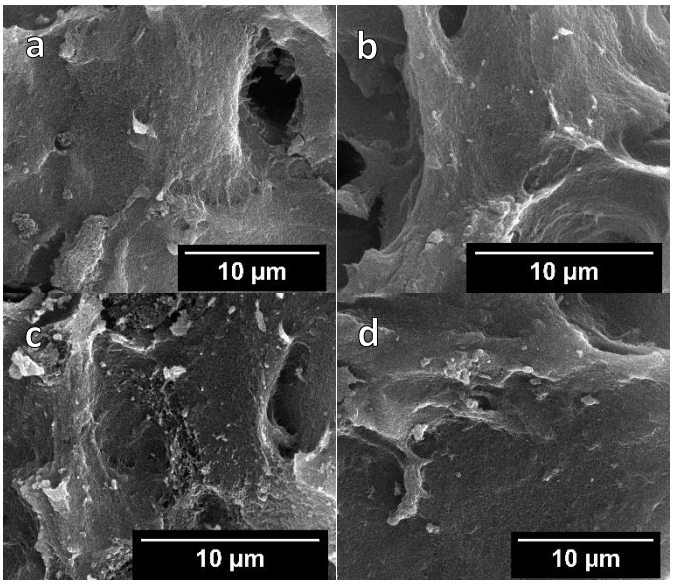

Figure 1: SEM images of carbogels treated at 1000 °C under inert nitrogen atmosphere (a) or under a mix of nitrogen and air, corresponding to an oxygen content of 1% (b), 2% (c) or 4% (d).

Table 1: Surface area, total pore volume, micro- and mesopore volume and yield of nitrogen doped cryogel (HTC) and carbogels treated at 1000 °C under either pure nitrogen atmosphere or a mixture of nitrogen and compressed air.

Sample	S_{BET} [m^2 g^{-1}]	V_{tot} [cm^3 g^{-1}]	V_{meso} [cm^3 g^{-1}]	V_{micro} [cm^3 g^{-1}]	Yield [%]
CN-HTC	101	0.640	0.640	0	-
CN-N_2	110	0.300	0.283	0.017	42.3
CN-1% O_2	634	0.552	0.353	0.199	39.1
CN-2% O_2	874	0.594	0.303	0.291	33.1
CN-4% O_2	1150	0.824	0.445	0.379	29.8

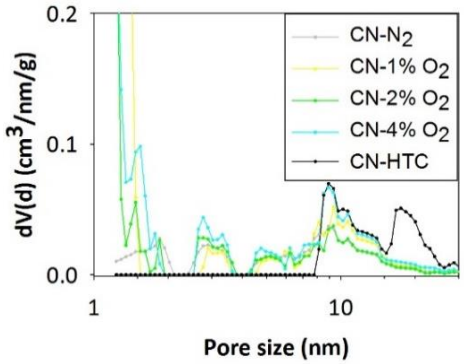

Figure 2: Pore size distribution of a nitrogen doped cryogel (HTC) and carbogels treated at 1000°C under either pure nitrogen atmosphere or a mixture of nitrogen and compressed air.

CN-HTC only consist of mesopores between 7 and 30 nm, while all carbonised samples also exhibit mircopores, where the micropore volume increases with increasing oxygen content. A similar trend can be seen in the elemental composition (Table 2) determined via XPS, where the carbon content decreases, due to *hole burning* with increasing oxygen percentage during the carbonisation, while the incorporated oxygen content itself is increased. The highest amount of nitrogen can be found in CN-N_2 with 3.3 at%, which reduces to 2.9 at% and 1.8 at% in CN-1% O_2 and CN-2% O_2, respectively. This can be expected as nitrogen is incorporated within the carbon framework, parts of it will be lost through *hole burning*, in a similar way to C atoms, creating NO and NO_2. Contrary to expectations, the nitrogen content rises again in CN-4% O_2 to 2.4 at%, where at the same time the composition of nitrogen and oxygen species is changed. C1s spectra and peak positions/fractions are similar for all samples, CN-4% O_2 exhibits an additional peak in the O1s spectra at 536 eV, which can be assigned to adsorbed water. While the other three samples consist of mostly graphitic N (59-66 %), followed by pyridinic (26-34 %) and N-oxides (6-11 %), CN-4% O_2 also shows pyrrolic N (30 %), which drastically reduces the percentage of graphitic N to 30 %. We assume that this change in elemental composition might be caused by interactions with other components present in compressed air, which was used to create the mix of N_2/O_2 during carbonisation. Detailed XPS spectra, peak positions and fractions of species as well as deconvoluted C1s, O1s and N1s spectra can be found in the ESI. Elemental composition of the bulk material determined via elemental analysis for CN-HTC and CN-1% O_2 is in good agreement with values obtained via XPS and indicates a homogeneous distribution of nitrogen throughout the materials bulk and surface.

Electrochemical testing was carried out in alkaline conditions with an RRDE setup for all four samples and compared to a commercially available platinum standard. The resulting voltammograms are show in Figure 3. CN-2% O_2 and CN-4% O_2 show the most positive onset potential, while CN-2% O_2 has the lowest limiting current of all four samples. The better performance of CN-2% O_2 compared to CN-N_2 and CN-1% O_2 might be attributed to the higher surface area, while the slight advantage over CN-4% O_2 which has a higher surface area and

Table 2: Elemental composition determined by XPS in at%/*EA in wt%* of a nitrogen doped cryogel (HTC) and carbogels treated at 1000 °C under either pure nitrogen atmosphere or a mixture of nitrogen and compressed air. N1 = pyridinic N (~398.1 eV), N2 = graphitic N (~400.7 eV), N3 = N-oxides (~403 eV), N4 = pyrrolic N (~399.7 eV) in fractions (%).

Sample	C	O	N	N1	N2	N3	N4
CN-HTC	79.8/ *63.5*	16.2 -	4.0/ *5.0*	11	12	2	75
CN-N_2	92.3	4.4	3.3	30	59	11	-
CN-1% O_2	91.8/ *88.6*	5.3 -	2.9/ *2.9*	26	66	8	-
CN-2% O_2	91.2	7.0	1.8	31	60	9	-
CN-4% O_2	89.6	8.0	2.4	34	30	6	30

nitrogen content, might be assigned to the difference in nitrogen speciation, with a similar amount of pyridinc N, but twice the amount of graphitic N. Lai et al.[13] reported that pyridinic N might contribute to the onset potential, while graphitic N might determine the limiting current. A study by Kim et al.[34] suggested that the outermost graphitic N represent the most active catalytic sites, but are converted into pyridinic N after one catalytic cycle, thus making both N species active. Considering that pyrrolic N does not represent an active site for the ORR, CN-4% O_2 has a similar amount of active nitrogen species (1.68 at% compared to 1.8% in CN-2% O_2), though differently distributed with 34% and 30% of pyridinic and graphitic N (compared to 30% and 60% in CN-2% O_2), respectively. At the same time CN-4% O_2 has a higher surface area of 1150 m^2 g^{-1} compared to 874 m^2 g^{-1} for CN-2% O_2, making their overall catalytic performance similar (LSV, electron transfer number and H_2O_2 yield). Average electron transfer numbers and H_2O_2 yields are similar for all four samples with values of 3 (49.6 %), 3.2 (38.5 %), 3.1 (42.4 %) and 3.1 (43.2 %) for CN-N_2, CN-1% O_2, CN-2% O_2 and CN-4% O_2, respectively.

Overall it can be concluded that O_2 activation during high temperature carbonisation represents an easy and more sustainable way, compared to harsh chemical activation, to tuning surface area, pore properties and elemental composition of biomass derived carbogels.

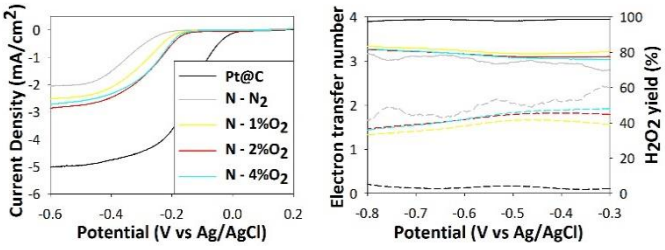

Figure 3: Linear sweep voltammogram recorded in 0.1 M KOH with an RRDE setup at 1600 rpm and electron transfer number and hydrogen peroxide yield of a commercially available platinum catalyst (60 wt% Pt@C) and carbogels treated at 1000 °C under either pure nitrogen atmosphere or a mixture of nitrogen and compressed air.

Influence of sulphur and boron incorporation

Co-doping of nitrogen and sulphur (CN_S), as well as nitrogen and boron (CN_B), and triple doping of nitrogen, sulphur and boron (CN_{SB}) were investigated. Based on the findings of the O_2 activation study, all carbonisations were carried out under a nitrogen atmosphere mixed with compressed air corresponding to 2 % of oxygen. This ratio was chosen due to its beneficial effect on the surface area, pore properties and ORR performance without substantial yield loss (< 30 %).

Scanning and Transmission electron micrographs, as well as BET surface areas, total pore volumes, meso- and micropore volumes of a pure carbogel and the three doped versions are shown in Figure 4 and Table 3, respectively. Nitrogen sorption isotherms can be found in the ESI. Additional doping of the nitrogen carbogel results in a decrease in surface area for all three samples, where the incorporation of boron seems to also affect the materials morphology. While the incorporation of sulphur does not greatly interfere with the formation of the carbogel structure, it limits the surface area to 692 ± 6 $m^2 g^{-1}$, compared to 889 ± 25 $m^2 g^{-1}$ in the pure N doped carbogel CN, and decreases the nitrogen content from 4 at% to 2.9 at%. A similar trend was observed by Wohlgemuth et. al.[14], where they concluded that the incorporation of sulphur, from TCA as a precursor, only occurs via electrophilic aromatic substitution or cycloadditon, suggesting that the crosslinking process during the aerogel formation remains unaffected. However, the incorporation of boron changes the overall morphology of the carbogel by creating a particle-like structure for both boron doped samples, CN_B and CN_{SB}, compared to a more rod-like structure, as in the case of CN and CN_S. This change is also reflected in the decrease of surface area and pore volume for CN_B and CN_{SB} to 669 ± 29 $m^2 g^{-1}$ and 605 ± 18 $m^2 g^{-1}$, respectively, while again the presence of TCA as a sulphur precursor reduced the surface area compared to CN_B. The changes in morphology suggest that the incorporation of boron interferes with the formation of the cryogel structure. Boric acid and borax have

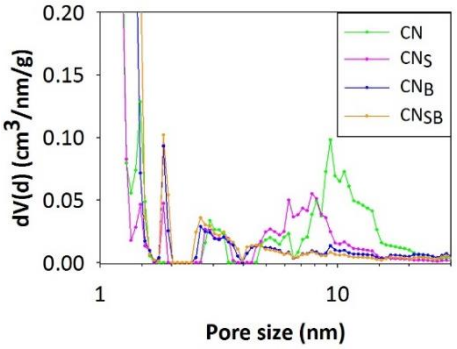

Figure 5: Pore size distributions of nitrogen carbogels, CN, treated at 1000 °C doped with sulphur CN_S, boron CN_B, and sulphur and boron CN_{SB}.

been shown to catalyse hexoses, such as glucose or fructose to HMF during hydrothermal carbonisation.[21,35] This can be explained by a change in reactivity and physical properties of the sugar solution due to negatively charged borate diol/didiol complexes.[26,36,37] Fellinger et al.[21,38] reported the synthesis of carbogels made purely from hydrothermally treated glucose and borax with a similar morphology to CN_B and CN_{SB} (Figure 4e/f and g/h). Considering these findings, we suggest that the catalytic effect of BA determines the structure instead of the presence of OvA, creating an altered cryogel architecture. Apart from the visual evidence, this assumption is also supported by the difference in pore properties, which can be seen in Figure 5. All carbogels show similar features in the micro- and small mesoporous region, whereas CN and CN_S also exhibit larger mesopores in the region of 5-20 nm. In addition to changing the carbogels morphology and pore properties, the presence of BA also helps promote the incorporation of a higher nitrogen content (4 at% for CN and 5.1/5.5 at% for CN_B/CN_{SB}), as can be seen from the elemental composition determined via XPS (detailed XPS spectra in ESI) in Table 4. This might be due to changes in the cryogel structure caused by BA, leaving OvA to

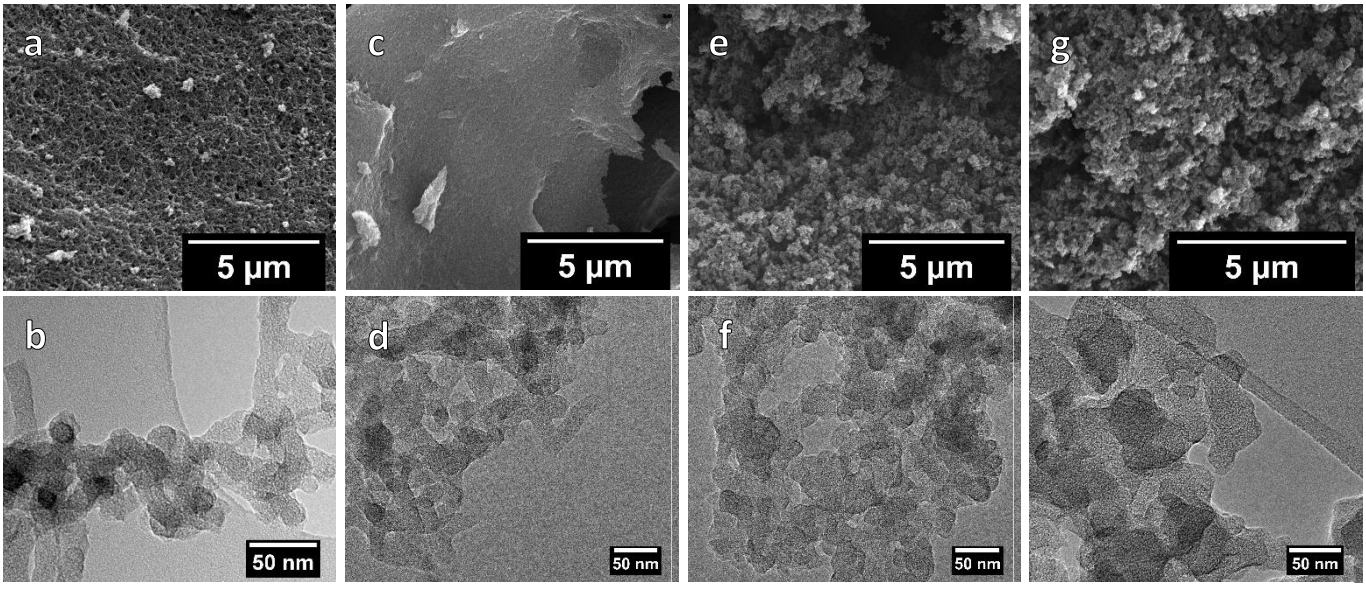

Figure 4: SEM and TEM images of nitrogen carbogels CN (a/b) treated at 1000 °C doped with sulphur CN_S (c/d), boron CN_B (e/f) and sulphur and boron CN_{SB} (g/h)

Table 3: Surface area, total pore, meso- and micropore volume of N doped and N/S/B doped carbogels treated at 1000 °C as average values for three independent carbonisations.

Sample	Surface area [$m^2\ g^{-1}$]	V_{tot} [$cm^3\ g^{-1}$]	V_{meso} [$cm^3\ g^{-1}$]	V_{micro} [$cm^3\ g^{-1}$]
CN	889 ± 25	0.770 ± 0.046	0.489 ± 0.056	0.281 ± 0.010
CN_S	692 ± 6	0.503 ± 0.013	0.279 ± 0.012	0.224 ± 0.003
CN_B	669 ± 29	0.488 ± 0.053	0.266 ± 0.047	0.222 ± 0.010
CN_{SB}	605 ± 18	0.412 ± 0.031	0.209 ± 0.035	0.203 ± 0.007

be fully utilised as a nitrogen source instead of also acting as structure directing/surface stabilising agent. Unlike the borax mediated carbogels,[21,22] we were also able to incorporate small amounts of boron (0.8 at% for CN_B and 0.5 at% for CN_{SB}) into the carbon framework using BA. The sulphur content was seen to be marginally higher (0.8 at% for CN_S and 1 at% for CN_{SB}) in the presence of BA. C1s and O1s photoelectron spectra (Figure S7) show similar peaks and fractions for all species (Table S2). N1s photoelectron spectra and the deconvoluted N species for all four samples can be seen in Figure 6, where N1 corresponds to pyridinic N, N2 to graphitic N and N3 to N-oxides, which are assigned to peaks around 398.1 eV, 400.7 eV and 403 eV, respectively.[39] Fractions of the three N species in all four samples can be found in Table 4. Compared to CN and CN_S, CN_B and CN_{SB} show almost identical distribution of N species, with 58 % of graphitic and 33 or 32 % of pyridinic N, indicating again that the addition of BA yields a different cryogel morphology/ composition. CN_S exhibits a lower pyridinic N content, which is compensated by a higher amount of graphitic N, as well as having a lower overall nitrogen content compared to CN, CN_B and CN_{SB}. This suggests that the addition of TCA does not interfere with the cryogel formation itself, but with the incorporation of nitrogen. Due to very low amounts of boron doping no B-C (282.4 – 283.2 eV) or B-N (397.8 eV) peaks[40,41] could be detected in C1s or N1s spectra for CN_B and CN_{SB}. Furthermore, deconvolution of B1s and S2p photoelectron spectra was not possible due to the low amounts of dopant, resulting in no information on how sulfur or boron are incorporated into the carbon framework.

Electrochemical testing was carried out in the form of linear sweep voltammetry and chronoamperometry for all four samples and compared to a platinum standard (Figure 7). All carbogels are clearly outperformed by platinum on carbon in

Table 4: Elemental composition determined by XPS in at% for carbogels treated at 1000 °C. N1 = pyridinic N (~398.1 eV), N2 = graphitic N (~400.7 eV), N3 = N-oxides (~403 eV) in fractions (%).

Sample	C	O	N	S	B	N1	N2	N3
CN	78.1	17.9	4.0	-	-	32	55	13
CN_S	83.4	12.9	2.9	0.8	-	23	65	12
CN_B	80.1	14.0	5.1	-	0.8	33	58	9
CN_{SB}	80.1	12.9	5.5	1.0	0.5	32	58	10

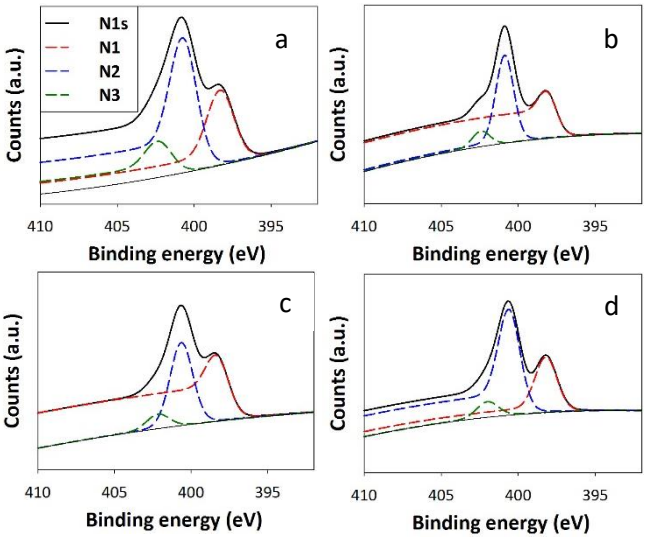

Figure 6: Deconvoluted N1s photoelectron envelope with nitrogen species (dashed lines), N1/red = pyridinic N, N2/blue = graphitic N, N3/green = N-oxides. For a) CN, b) CN_S, c) CN_B and d) CN_{SB}.

terms of catalytic activity, though they show a better long time stability with 85 % remaining for CN and CN_B, 82 % for CN_{SB} and 80 % for CN_S after 10000 s. The onset potential increases in the order CN > CN_B > CN_{SB}/CN_S, while the limiting current is lowest for CN_{SB}, followed by CN_B, CN and CN_S. Relating the linear sweep voltammograms to the elemental composition of the samples, it appears that the nitrogen content is the critical parameter when it comes to the limiting current, while the oxygen content might have an influence on the onset potential. In contrast to Wohlgemuth et al.,[14] who observed improved catalytic activity when co-doping N and S, CN_S exhibits the worst performance amongst the present samples, indicating that additional sulphur doping does not appear to have a beneficial influence on the overall morphology or catalytic activity of the studied carbogels. Although the NS co-doped aerogel of Wohlgemuth et al.[14] had similar levels of N and S doping and exhibited comparable onset potential and limiting current to the CN_S sample in the present work it had lower surface area and pore volume (224 $m^2\ g^{-1}$ and 0.27 $cm^3\ g^{-1}$). The incorporation of boron seems to play a crucial role, with CN_B and CN_{SB} showing the best electron transfer numbers and hydrogen peroxide yields, where CN_B has the highest and lowest value with 3.5 and 22.6 %, respectively, showing a significant improvement compared to the pure CN carbogel with a H_2O_2 yield of 44.7 %. All carbogels appear to proceed via a mixture of the 2- and 4-electron pathway with electron transfer numbers between 3.0 and 3.5, and H_2O_2 yields between 22.6 - 48.4 % (Table S3). Based on our results, we assume a synergistic effect of nitrogen and boron which contributes towards the slightly superior performance of CN_B and CN_{SB}. Similar findings were reported by other researchers, which observed catalytically improved performance of N/B co-doped samples compared to their single-doped counterparts.[42–45] Zheng et al.[42] investigated the synergistic effect of N and B co-doping via DFT calculations, concluding that a B atom *meta* to a pyridinic N atom, forming a B-C-N heteroring, is more active

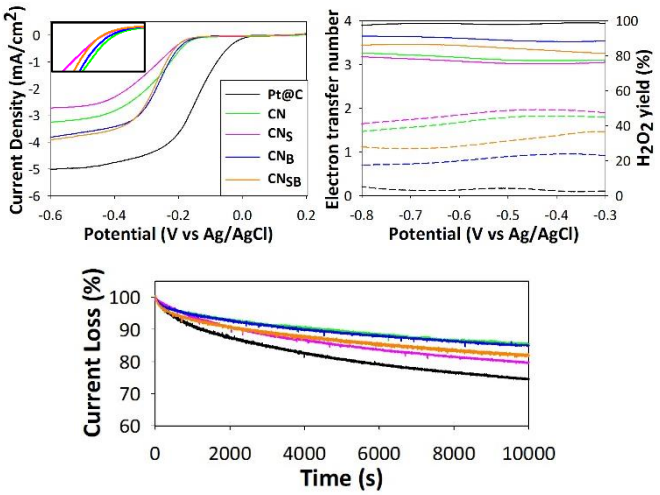

Figure 7: Linear sweep voltammogram recorded in 0.1 M KOH with an RDE setup at 1600 rpm, electron transfer number and hydrogen peroxide yield and chronoamperometric response at a constant potential of 0.25 V (vs Ag/AgCl) for a commercially available platinum catalyst (60 wt% Pt@C) and nitrogen carbogels, CN, treated at 1000 °C doped with sulphur, CN_S, boron, CN_B, or sulphur and boron, CN_{SB}.

than an *ortho* B atom directly bonded to a pyridinic or graphitic N, forming a NB functionality. They suggested that the in between C atom can be polarised by the N atom, to then donate extra electrons to the B atom, which will improve its oxygen adsorption properties and make it an active site. Contrary to Wohlgemuth et al.,[22] who studied the influence of surface area on borax mediated N doped carbogels, we were not able to identify a clear correlation between surface area/pore properties and the catalytic performance of our studied carbogels. Whereas we observed that heteroatom doping, especially N and B co-doping, as well as the nitrogen content itself, has a much stronger impact. Our samples show similar, though slightly lower, performance compared to their best performing sample, which had a similar nitrogen (4.5 wt%), but lower oxygen (3.1 wt%) content to our boron doped samples, with a lower surface area of 265 $m^2 g^{-1}$. However, they detected 35 ppm of iron originating from borax residues in their sample, which might have contributed to their sample's superior performance, especially in terms of limiting current, as it has been shown that even traces as low as 18 ppm of metals can change the catalytic activity.[46] In the present study, nitrogen speciation does not seem to greatly influence catalytic activity. However, fractions of N species in the studied samples are too similar to conclusively support the findings of Kim et al.[34] that both, pyridinic and graphitic N are active sites.

Conclusions

The easy tunablity/adjustability of sustainable and inexpensive nitrogen carbogels derived via a simple one-pot synthesis by environmentally friendly physical activation or heteroatom doping has been demonstrated. Oxygen activation during high temperature carbonisation at 1000 °C increased the carbogel surface area and micropore volume up to 1150 $m^2 g^{-1}$, while incorporating higher amounts of oxygen but with decreased yield due to O_2 etching of C and N atoms. The best catalytic performance was recorded for a sample carbonised under nitrogen atmosphere mixed with 2% of oxygen, though exhibiting a lower surface area of only 874 $m^2 g^{-1}$, by having a more beneficial ratio of graphitic and pyridinic N, which are considered as active sites.

Additional heteroatom doping of a nitrogen carbogel with sulphur did not result in an increased catalytic performance due to a decrease in surface area and nitrogen content. The addition of boric acid yielded differently structured cryogels, with lower surface area than the pure nitrogen carbogel, where it is proposed that boric acid acts as a structure directing agent during the formation of the cryogel, rather than ovalbumin, allowing for the protein to act as more efficient nitrogen source resulting in higher N content. The main active sites are pyridinic and/or graphitic nitrogen atoms, which seem to influence the limiting current, while the oxygen content seems to influence the onset potential. An assumed synergistic effect between N and B enables superior catalytic activity with the highest electron transfer number of 3.5 and lowest H_2O_2 yield of only 22.6 %.

Though the carbogels studied in the present work have poorer performance than a commercial platinum standard, superior stability in alkaline media has been shown and they are similar in performance to other truly metal-free catalysts. The study indicates that key properties such as carbogel structure, surface area, pore properties and dopant level can be controlled to improve performance. The sustainable approach presented here may be adopted in materials for other energy applications such as supercapacitors or batteries, where surface area and pore properties also play a crucial role.

Acknowledgements

Kathrin Preuss would like to thank the Materials Research Institute of Queen Mary, University of London for a PhD studentship. Liviu C. Tănase and Cristian M. Teodorescu acknowledge funding from the UEFISCDI Agency through the Project PN-II-RU-TE-2014-4-0456 and by the NIMP Core Project PN16-48012, both projects being granted by the Romanian Ministry of Research and Innovation.

Notes and references

1 I. Katsounaros, W. B. Schneider, J. C. Meier, U. Benedikt, P. U. Biedermann, A. a. Auer and K. J. J. Mayrhofer, *Phys. Chem. Chem. Phys.*, 2012, **14**, 7384.

2 L. Zhang and Z. Xia, *J. Phys. Chem. C*, 2011, **115**, 11170–11176.

3 N. Daems, X. Sheng, I. F. J. Vankelecom and P. P. Pescarmona, *J. Mater. Chem. A*, 2014, **2**, 4085.

4 J. Liu, P. Song, Z. Ning and W. Xu, *Electrocatalysis*, 2015, **6**, 132–147.

5 L. Dai, Y. Xue, L. Qu, H.-J. Choi and J.-B. Baek, *Chem. Rev.*,

2015, **115**, 4823–4892.
6 M. Shao, Q. Chang, J.-P. Dodelet and R. Chenitz, *Chem. Rev.*, 2016, **116**, 3594–3657.
7 P. He, M. Lefevre, G. Faubert and J. Dodelet, *J. new Mater. Electrochem. Syst.*, 1999, **2**, 243–252.
8 J. Masa, A. Zhao, W. Xia, Z. Sun, B. Mei, M. Muhler and W. Schuhmann, *Electrochem. commun.*, 2013, **34**, 113–116.
9 K. Gong, F. Du, Z. Xia, M. Durstock and L. Dai, *Science (80-.).*, 2009, **323**, 760–764.
10 Y. Shao, J. Sui, G. Yin and Y. Gao, *Appl. Catal. B Environ.*, 2008, **79**, 89–99.
11 K. R. Lee, K. U. Lee, J. W. Lee, B. T. Ahn and S. I. Woo, *Electrochem. commun.*, 2010, **12**, 1052–1055.
12 H. Niwa, K. Horiba, Y. Harada, M. Oshima, T. Ikeda, K. Terakura, J. I. Ozaki and S. Miyata, *J. Power Sources*, 2009, **187**, 93–97.
13 L. Lai, J. R. Potts, D. Zhan, L. Wang, C. K. Poh, C. Tang, H. Gong, Z. Shen, J. Lin and R. S. Ruoff, *Energy Environ. Sci.*, 2012, **5**, 7936.
14 S.-A. Wohlgemuth, R. J. White, M.-G. Willinger, M.-M. Titirici and M. Antonietti, *Green Chem.*, 2012, **14**, 1515.
15 J. P. Paraknowitsch and A. Thomas, *Energy Environ. Sci.*, 2013, **6**, 2839.
16 P. Chen, L.-K. Wang, G. Wang, M.-R. Gao, J. Ge, W.-J. Yuan, Y.-H. Shen, A.-J. Xie and S.-H. Yu, *Energy Environ. Sci.*, 2014, **7**, 4095–4103.
17 H. Zhang, Y. Wang, D. Wang, Y. Li, X. Liu, P. Liu, H. Yang, T. An, Z. Tang and H. Zhao, *Small*, 2014, **10**, 3371–3378.
18 K. Preuss, V. K. Kannuchamy, A. Marinovic, M. Isaacs, K. Wilson, I. Abrahams and M.-M. Titirici, *J. Energy Chem.*, 2016, **25**, 228–235.
19 H. W. Liang, Z. Y. Wu, L. F. Chen, C. Li and S. H. Yu, *Nano Energy*, 2015, **11**, 366–376.
20 N. Brun, S. A. Wohlgemuth, P. Osiceanu and M. M. Titirici, *Green Chem.*, 2013, **15**, 2514.
21 T. P. Fellinger, R. J. White, M. M. Titirici and M. Antonietti, *Adv. Funct. Mater.*, 2012, **22**, 3254–3260.
22 S.-A. Wohlgemuth, T.-P. Fellinger, P. Jäker and M. Antonietti, *J. Mater. Chem. A*, 2013, **1**, 4002.
23 R. J. White, N. Yoshizawa, M. Antonietti and M.-M. Titirici, *Green Chem.*, 2011, **13**, 2428.
24 N. Baccile, M. Antonietti and M.-M. Titirici, *ChemSusChem*, 2010, **3**, 246–253.
25 S.-M. Alatalo, K. Qiu, K. Preuss, A. Marinovic, M. Sevilla, M. Sillanpää, X. Guo and M.-M. Titirici, *Carbon N. Y.*, 2016, **96**, 622–630.
26 M.-M. TITIRICI, *Sustainable Carbon Materials from Hydrothermal Processes*, John Wiley & Sons, Ltd, Oxford, UK, 2013.
27 H. Nursten, *The Maillard Reaction: Chemistry, Biochemistry and Implications*, 2005.
28 J. Fan, M. Yudasaka, J. Miyawaki, K. Ajima, K. Murata and S. Iijima, *J. Phys. Chem. B*, 2006, **110**, 1587–1591.
29 R. T. Yang and C. Wong, *Science (80-.).*, 1981, **214**, 437–438.
30 R. T. Yang and C. Wong, *J. Chem. Phys.*, 1981, **75**, 4471–4476.
31 X. Chu and L. D. Schmidt, *Surf. Sci.*, 1992, **268**, 325–332.
32 A. N. Hayhurst and M. S. Parmar, *Chem. Eng. Sci.*, 1998, **53**, 427–438.
33 X. Chu and L. D. Schmidt, *Carbon N. Y.*, 1991, **29**, 1251–1255.
34 H. Kim, K. Lee, S. I. Woo and Y. Jung, *Phys. Chem. Chem. Phys.*, 2011, **13**, 17505.
35 T. S. Hansen, J. Mielby and A. Riisager, *Green Chem.*, 2011, **13**, 109.
36 M. Levy and E. A. Doidy, *J. Biol. Chem.*, 1929, **84**, 749–762.
37 J. M. Conner and V. C. Bulgrin, *J. Inorg. Nucl. Chem.*, 1967, **29**, 1953–1961.
38 S.-A. Wohlgemuth, T.-P. Fellinger, P. Jäker and M. Antonietti, *J. Mater. Chem. A*, 2013, **1**, 4002–4009.
39 B. J. Matsoso, K. Ranganathan, B. K. Mutuma, T. Lerotholi, G. Jones and N. J. Coville, *RSC Adv.*, 2016, **6**, 106914–106920.
40 X. Chen, Z. Wang, S. Ma and V. Ji, *Diam. Relat. Mater.*, 2010, **19**, 1336–1340.
41 C. Xu, Y. Su, D. Liu and X. He, *Phys. Chem. Chem. Phys.*, 2015, **17**, 25440–25448.
42 Y. Zheng, Y. Jiao, L. Ge, M. Jaroniec and S. Z. Qiao, *Angew. Chemie - Int. Ed.*, 2013, **52**, 3110–3116.
43 Y. Gong, H. Fei, X. Zou, W. Zhou, S. Yang, G. Ye, Z. Liu, Z. Peng, J. Lou, R. Vajtai, B. I. Yakobson, J. M. Tour and P. M. Ajayan, *Chem. Mater.*, 2015, **27**, 1181–1186.
44 J. S. Han, D. Y. Chung, D. G. Ha, J. H. Kim, K. Choi, Y. E. Sung and S. H. Kang, *Carbon N. Y.*, 2016, **105**, 1–7.
45 J. Tai, J. Hu, Z. Chen and H. Lu, *RSC Adv.*, 2014, **4**, 61437–61443.
46 L. Wang, A. Ambrosi and M. Pumera, *Angew. Chemie - Int. Ed.*, 2013, **52**, 13818–13821.

Electronic Supplementary Information

Sustainable metal-free carbogels as oxygen reduction electrocatalysts

K. Preuss,[a,b] L. C. Tănase,[c] C. M. Teodorescu,[c] I. Abrahams[b,d] and M.-M. Titirici[a,b]

[a] School of Engineering and Materials Science, Queen Mary University of London, Mile End Road, E1 4NS London, United Kingdom.

[b] Materials Research Institute, Queen Mary University of London, Mile End Road, E1 4NS London, United Kingdom.

[c] National Institute of Materials Physics, Atomistilor 405A, 077125 Măgurele-Ilfov, Romania.

[d] School of Biological and Chemical Sciences, Queen Mary University of London, Mile End Road, E1 4NS London, United Kingdom.

Email: m.m.titirici@qmul.ac.uk

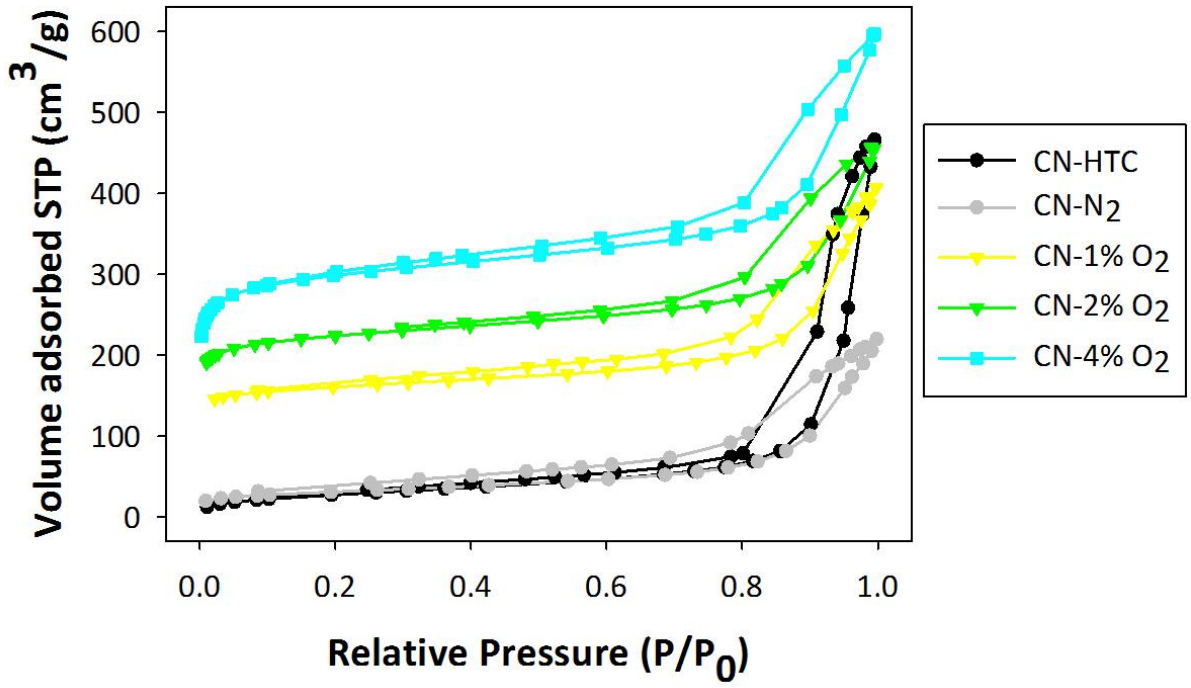

Figure S1: Nitrogen sorption isotherms at -196 °C of a nitrogen doped aerogel (CN-HTC) and carbogels treated at 1000°C under either pure nitrogen atmosphere (CN-N2) or a mixture of nitrogen and oxygen (CN-1% O_2, CN-2% O_2, CN-4% O_2).

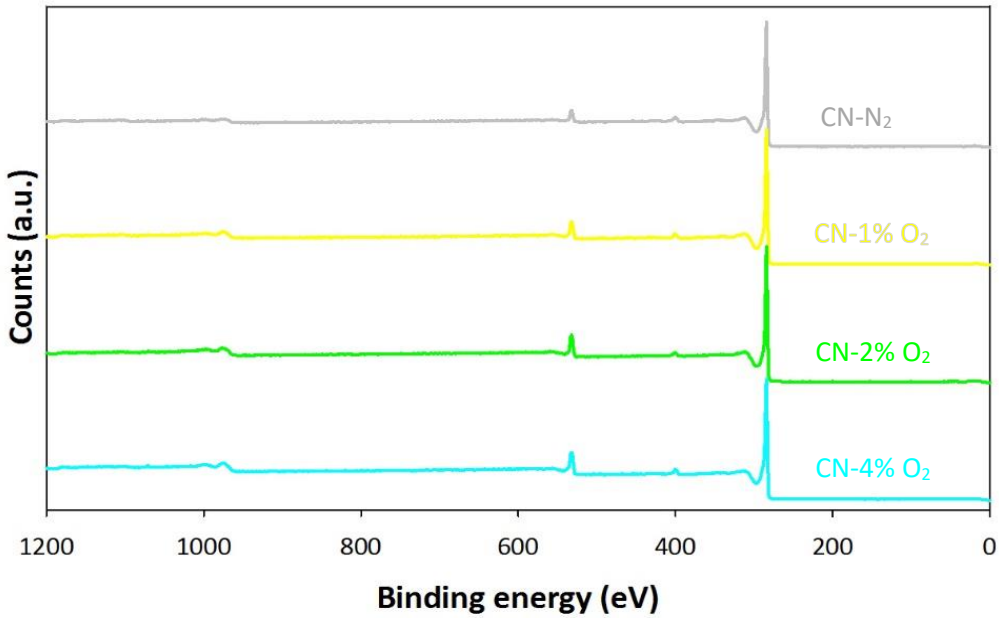

Figure S2: X-ray photoelectron spectra for nitrogen doped carbogels treated at 1000°C under either pure nitrogen atmosphere (CN-N_2) or a mixture of nitrogen and oxygen (CN-1% O_2, CN-2% O_2, CN-4% O_2).

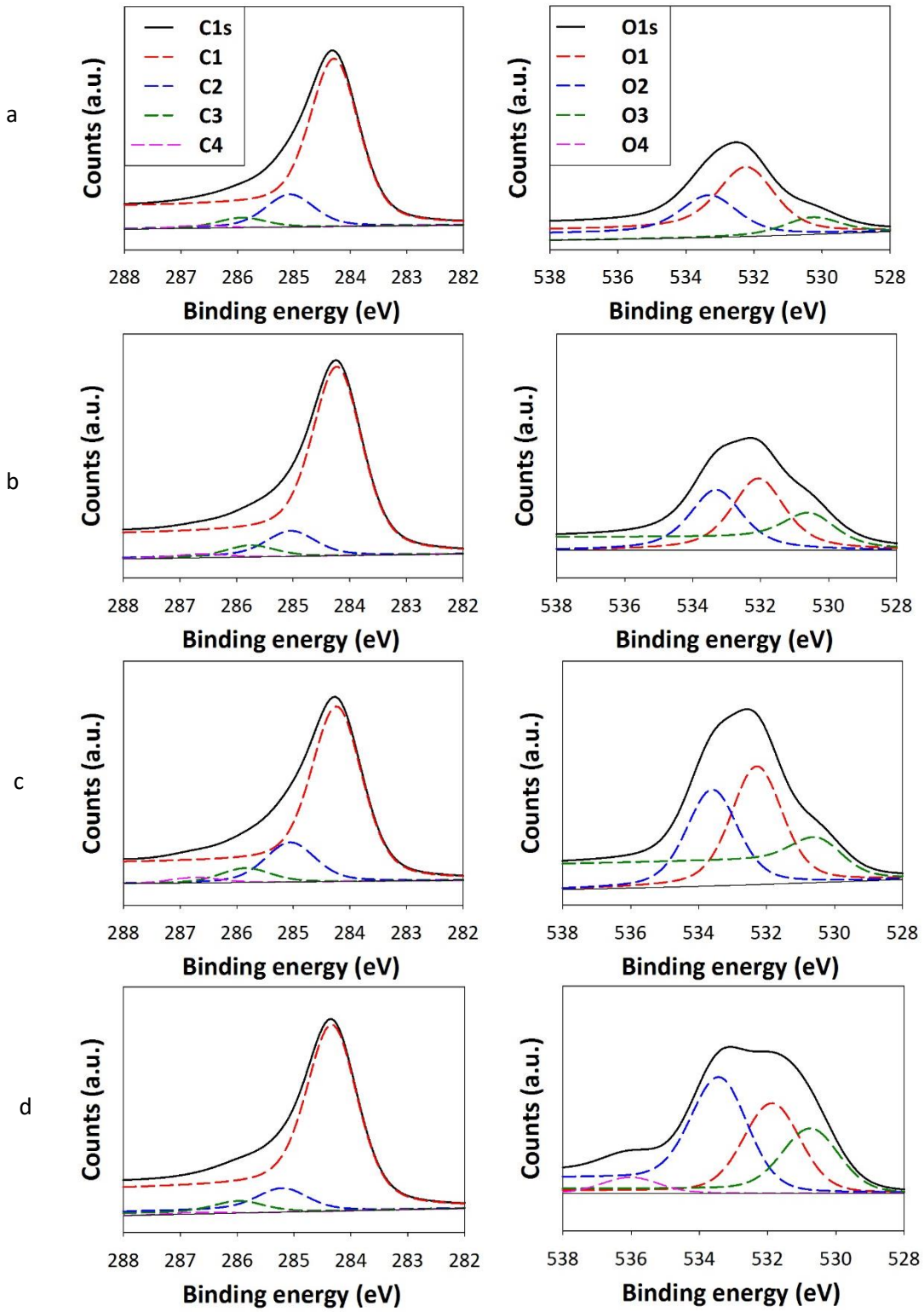

Figure S3: Deconvoluted C1s (left) and O1s (right) spectra for nitrogen doped carbogels treated at 1000°C under a) either pure nitrogen atmosphere (CN-N_2) or a mixture of nitrogen and oxygen b) CN-1% O_2, c) CN-2% O_2 and d) CN-4% O_2.

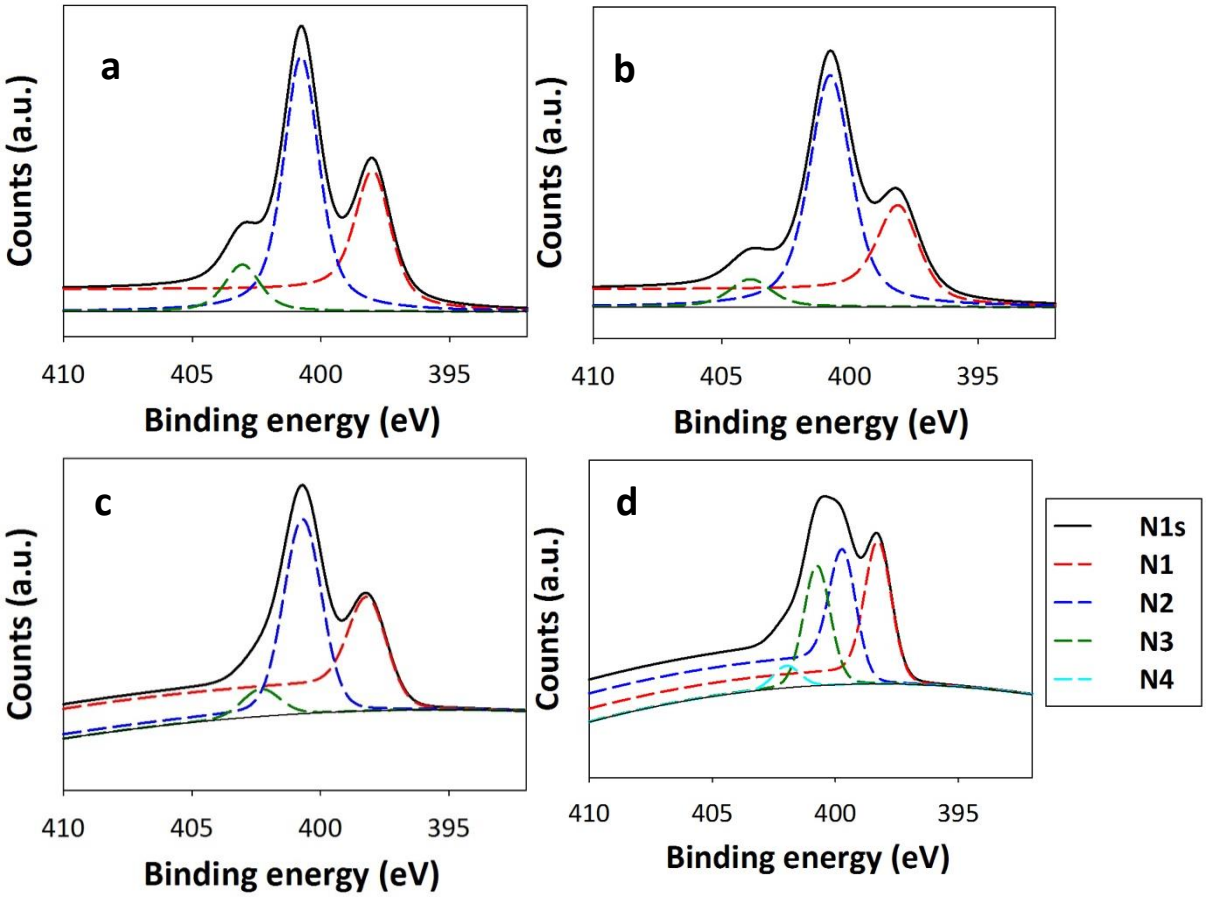

Figure S4: Deconvoluted N1s spectra for nitrogen doped carbogels treated at 1000°C under a) either pure nitrogen atmosphere (CN-N_2) or a mixture of nitrogen and oxygen b) CN-1% O_2, c) CN-2% O_2 and d) CN-4% O_2.

Table S1 : Binding energy (eV)/fraction of species (%) and assignment of peaks[1–4] for nitrogen doped carbogels treated at 1000°C under either pure nitrogen atmosphere (CN-N_2) or a mixture of nitrogen and oxygen CN-1% O_2, CN-2% O_2 and CN-4% O_2.

Peaks	CN-N_2	CN-1% O_2	CN-2% O_2	CN-4% O_2	Assigned to
C1s	284.27/78	284.21/81	284.22/74	284.32/83	C–C/C=C
	285.07/16	285.04/12	285.05/18	285.19/11	C–OH/C–O–C
	285.93/5	285.75/5	285.84/6	285.96/5	C-N
	286.71/1	286.61/2	286.74/2	286.67/1	C-O
O1s	530.27/15	530.52/19	530.45/14	530.73/23	C=O
	532.20/55	532.06/44	532.29/48	531.87/32	C-O
	533.29/30	533.31/37	533.60/39	533.40/39	O=C-O
	-	-	-	536.03/6	adsorbed H_2O
N1s	397.97/30	398.10/26	398.14/31	398.26/34	Pyridinic N
	-	-	-	399.69/30	Pyrrolic N
	400.77/59	400.76/66	400.69/60	400.75/30	Graphitic N
	403.06/11	403.88/8	402.33/9	401.99/6	N-oxides

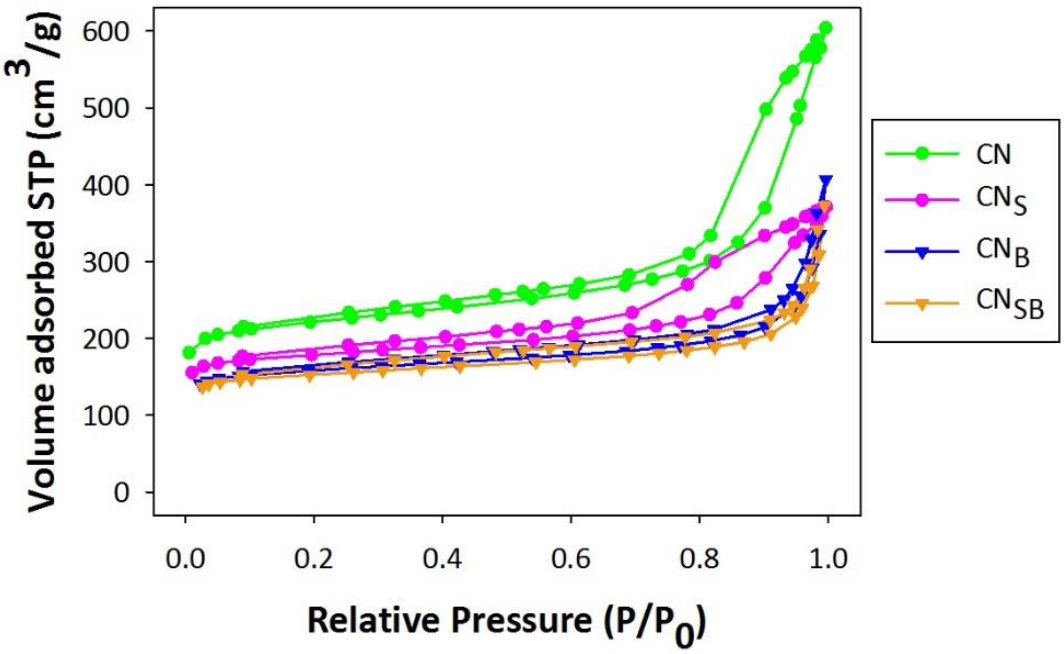

Figure S5: Nitrogen sorption isotherms at -196 °C of carbogels treated at 1000 °C doped with nitrogen (CN) and additional doping with sulfur (CN_S), boron (CN_B) and sulfur and boron (CN_{SB}).

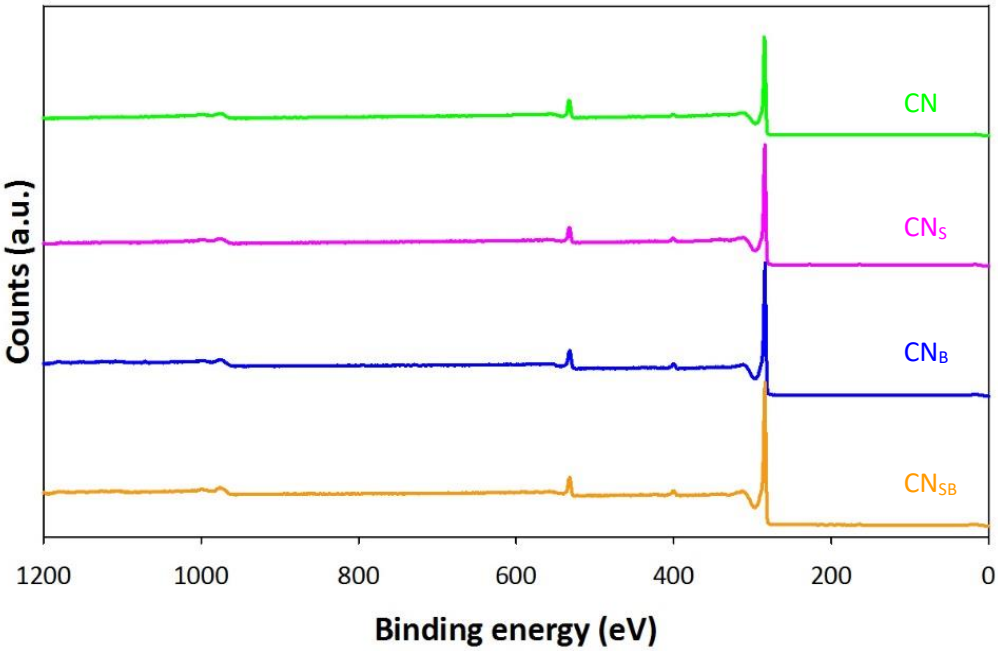

Figure S6: X-ray photoelectron spectra of carbogels treated at 1000 °C doped with nitrogen (CN) and additional doping with sulfur (CN_S), boron (CN_B) and sulfur and boron (CN_{SB}).

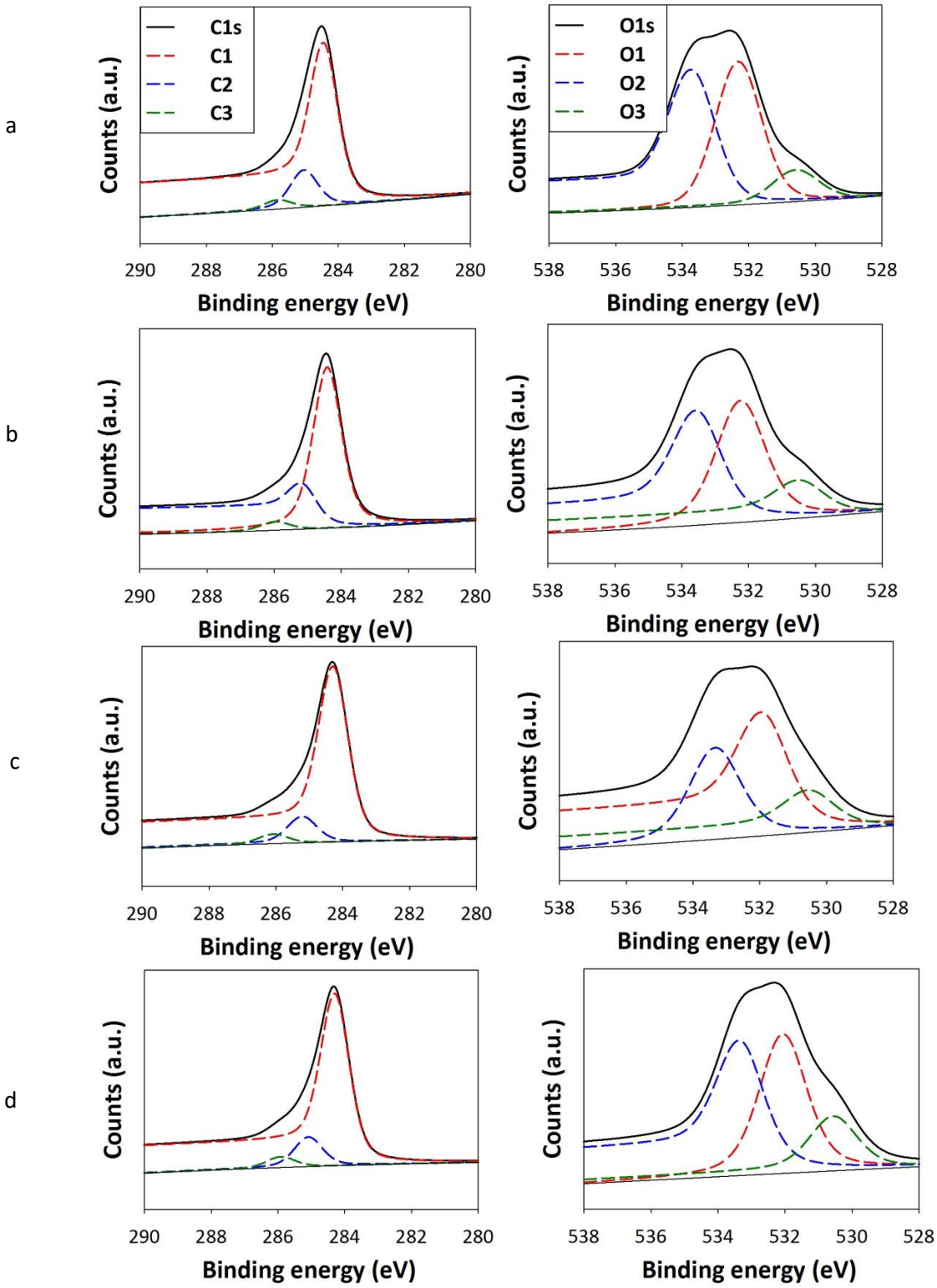

Figure S7: Deconvoluted C1s (left) and O1s (right) spectra for carbogels treated at 1000 °C doped with a) nitrogen (CN) and additional doping with b) sulfur (CN_S), c) boron (CN_B) and d) sulfur and boron (CN_{SB}).

Table S2: Binding energy (eV)/fraction of species (%) and assignment of peaks[1–4] for carbogels treated at 1000 °C doped with nitrogen (CN) and additional doping with sulfur (CN_S), boron (CN_B) and sulfur and boron (CN_{SB}).

Peaks	CN	CN_S	CN_B	CN_{SB}	Assigned to
C1s	284.43/76	284.41/80	284.27/82	284.28/80	C–C/C=C
	285.04/19	285.12/16	285.21/13	285.09/15	C–OH/C–O–C
	285.84/5	285.97/4	286.09/5	285.92/5	C-N/C-S
O1s	530.59/11	530.45/12	530.49/15	530.55/17	C=O
	532.31/48	532.24/48	531.89/45	532.06/45	C-O
	533.68/41	533.52/40	533.34/40	533.32/38	O=C-O
N1s	398.27/32	398.04/23	398.24/33	398.19/32	Pyridinic N
	400.68/55	400.88/65	400.64/58	400.58/58	Graphitic N
	402.28/14	402.44/12	402.17/9	402.01/10	N-oxides

Table S3: Electrochemical values derived from linear sweep voltammetry and chronoamperometry using an RRDE setup in 0.1 M KOH. Electron transfer number and H_2O_2 yield are averaged values between -0.3 V and -0.6 V.

Sample	**Onset potential @ -0.1 mA/cm² [V vs Ag/AgCl]**	**Limiting current @ -0.6 V [mA/cm²]**	**Electron transfer number**	**H_2O_2 yield [%]**	**Current after 10000 s [%]**
Pt@C	0.006	-5.0	3.9	3.3	75
CN	-0.133	-3.3	3.1	44.7	85
CN_S	-0.153	-2.7	3.0	48.4	80
CN_B	-0.143	-3.8	3.5	22.6	85
CN_{SB}	-0.158	-3.9	3.3	32.8	82

References:

1 C. H. Choi, S. H. Park and S. I. Woo, *Green Chem.*, 2011, **13**, 406–412.

2 A. Calborean, F. Martin, D. Marconi, R. Turcu, I. E. Kacso, L. Buimaga-Iarinca, F. Graur and I. Turcu, *Mater. Sci. Eng. C*, 2015, **57**, 171–180.

3 B. J. Matsoso, K. Ranganathan, B. K. Mutuma, T. Lerotholi, G. Jones and N. J. Coville, *RSC Adv.*, 2016, **6**, 106914–106920.

4 Z. Xing, Z. Ju, Y. Zhao, J. Wan, Y. Zhu, Y. Qiang and Y. Qian, *Sci. Rep.*, 2016, **6**, 26146.